Sensitivity of asymmetric Oxygen Minimum Zones to mixing intensity and stoichiometry in the tropical Pacific using a basin-scale model (OGCM-DMEC V1.4)

Kai Wang[1], Xiujun Wang[1,2*], Raghu Murtugudde[2], Dongxiao Zhang[3], Rong-Hua Zhang[4]

[1]College of Global Change and Earth System Science, Beijing Normal University, Beijing 100875, China
[2]Earth System Science Interdisciplinary Center, University of Maryland, College Park, Maryland 20740, USA
[3]JISAO, University of Washington and NOAA, Pacific Marine Environmental Laboratory, Seattle, Washington 98115, USA
[4]Institute of Oceanology, Chinese Academy of Sciences, Qingdao, Shandong 266071, China

Correspondence to: Xiujun Wang (xwang@bnu.edu.cn)

Abstract. The tropical Pacific Ocean holds the world's two largest Oxygen Minimum Zones (OMZs), showing a prominent hemispheric asymmetry, with a much stronger and broader OMZ north of the equator. However, many models have difficulties in reproducing the observed asymmetric OMZs in the tropical Pacific. Here, we apply a fully coupled basin-scale model to evaluate the impacts of stoichiometry and the intensity of vertical mixing on the dynamics of OMZs in the tropical Pacific. We first utilize observational data of dissolved oxygen (DO) to calibrate and validate the basin-scale model. Our model experiments demonstrate that enhanced vertical mixing combined with reduced O:C utilization ratio can significantly improve our model capability of reproducing the asymmetric OMZs. Our study shows that DO is more sensitive to biological processes over 200-700 m but to physical processes over 400-1000 m. Enhanced vertical mixing causes a large increase in physical supply and a small increase in biological consumption whereas applying a reduced O:C utilization ratio leads to a large decrease in biological consumption, and a small decrease in physical supply. Our analyses suggest that biological consumption (greater rate to the south) cannot explain the asymmetric feature in the tropical Pacific OMZs, but physical processes (stronger supply to the south) play a major role in regulating the asymmetry of the tropical Pacific's OMZs. This study also highlights the roles of physical and biological interactions/feedbacks in contributing to the asymmetry of OMZs in the tropical Pacific.

1 Introduction

Photosynthesis and respiration are important processes in all ecosystems on the Earth, with carbon and oxygen being the two main elements. The carbon cycle has garnered much attentions, with significant progress in both the observations and modelling of biological processes (e.g., uptake of CO_2 and respiration), and physical/chemical processes (e.g., carbon fluxes between the atmosphere, land and ocean). However, the oxygen cycle has received much less attention despite its large role in the earth system (Breitburg et al., 2018; Oschlies et al., 2018).

Dissolved oxygen (DO) is a sensitive indicator of physical and biogeochemical processes in the ocean thus a key parameter for understanding the ocean's role in the climate system (Stramma et al., 2010). In addition to photosynthesis and respiration, the distribution of DO in the world's oceans is also regulated by air-sea gas exchange, ocean circulation and ventilation (Bettencourt et al., 2015; Bopp et al., 2002; Levin, 2018). Unlike most dissolved nutrients that display an increase in concentration with depth, DO concentration is generally low at mid-depth of the ocean. The most remarkable feature in the oceanic oxygen dynamics is the so-called Oxygen Minimum Zone (OMZ) that is often present below 200 m in the open oceans (Karstensen et al., 2008; Stramma et al., 2008). Previous studies have used the isoline of 20 mmol m^{-3} as the boundary of the OMZ for the estimation of OMZ volume (Bettencourt et al., 2015; Bianchi et al., 2012; Fuenzalida et al., 2009), and also as an up limit to determine the suboxic water (Wright et al., 2012).

The world's two largest OMZs are observed in the Eastern Tropical North Pacific (ETNP) and South Pacific (ETSP), showing a peculiar asymmetric structure across the equator, i.e., a much larger volume of suboxic water (<20 mmol m^{-3}) to the north than to the south (Bettencourt et al., 2015; Paulmier and Ruiz-Pino, 2009). It is known that OMZs are caused by the biological consumption associated with remineralization of organic matter (OM), and weak physical supply of DO due to sluggish subsurface ocean circulation and ventilation (Brandt et al., 2015; Czeschel et al., 2011; Kalvelage et al., 2015). Although there have been a number of observation-based analyses addressing the dynamics of OMZs in the tropical Pacific during the past decade (Czeschel et al., 2012; Garçon et al., 2019; Schmidtko et al., 2017; Stramma et al., 2010), our understanding is limited on the underlying mechanisms that regulate DO dynamics at mid-depth (Oschlies et al., 2018; Stramma et al., 2012).

Large-scale physical-biogeochemical models have become a useful tool to investigate the potential sensitivity of OMZs to climate change (Duteil and Oschlies, 2011; Ward et al., 2018; Williams et al., 2014). However, many models have been unable to reproduce the observed patterns of asymmetric OMZs in the tropical Pacific (Cabre et al., 2015; Shigemitsu et al., 2017), which may be due to "unresolved ocean transport processes, unaccounted for variations in respiratory oxygen demand, or missing biogeochemical feedbacks" (Oschlies et al., 2018). A common problem is that the two asymmetric OMZs merge into one in most models due to overestimated OMZ volume in the tropical Pacific, which may be related to the regulation of physical supply and/or biological respiration demand (Cabre et al., 2015; Shigemitsu et al., 2017). Recent studies have also indicated that a realistic representation of circulation and ventilation processes with a high-resolution ocean model is critical to predict the asymmetric OMZs in the tropical Pacific (Berthet et al., 2019; Busecke et al., 2019). Hence, it's necessary to carry out model-data integrative studies to improve model capacity of simulating the dynamics of the tropical OMZs, and to better understand the relative roles of physical and biological processes. Without such process understandings, it is unclear a priori whether simply increasing resolution will render better simulations and predictions.

A basin-scale ocean general circulation model coupled with a dynamic marine ecosystem-carbon model (OGCM-DMEC) was developed for the tropical Pacific, which showed capability of reproducing observed spatial and temporal variations of physical, nutrient and carbon fields in the upper ocean (Wang et al., 2008; Wang et al., 2015; Wang et al., 2009b), and nitrate, iron, POC/detritus and export production below 200 m (Yu et al., 2021). In this study, we conduct model sensitivity experiments and evaluation on responses of mid-depth DO to parameterizations of two relevant processes (i.e., oxygen-restricted remineralization and vertical mixing). We first carry out model calibration and validation using observational data of basin-scale DO and oxygen consumption in the water column of the southern tropical Pacific to improve the simulation of OMZs in the tropical Pacific. Then, we analyse the impacts of new parameterizations on biological consumption and physical supply and their relative contributions to the dynamics of mid-depth DO. The objective of this study is to advance our model capacity to simulate the oceanic oxygen cycle, and to identify the mechanisms driving the asymmetric OMZs in the tropical Pacific.

2. Model description

2.1 Ocean physical model

The basin-scale OGCM, a reduced-gravity, primitive-equation, sigma-coordinate model, is coupled to an advective atmospheric model (Murtugudde et al., 1996). There are 20 layers with variable thicknesses and a total depth of ~1200 m in the OGCM. The mixed layer (the upper-most layer) depth is determined by the Chen mixing scheme (Chen et al., 1994), which varies from 10 m to 50 m on the equator. The remaining layers in the euphotic zone are approximately 10 m in thickness. The vertical resolution is approximately 30-50 m in the core OMZ (at ~300-500 m). The model domain is between 30ºS and 30ºN for the Pacific, and zonal resolution is 1º. Meridional resolution varies between 0.3º and 0.6º over 15ºS-15ºN (1/3° over 10°S-10ºN), and increases to 2º in the southern and northern "sponge layers" (the 25º-30º bands) where temperature, salinity, nutrients and DO are gradually relaxed back towards the observed climatological seasonal means. The model closes the western boundary and no representation of the Indonesian throughflow is included. The boundary conditions of temperature, salinity, nitrate and DO are from the World Ocean Atlas, 2013 (WOA2013: http://www.nodc.noaa.gov/OC5/woa13/pubwoa13.html), and boundary condition for dissolved iron is based on limited field data, and given by a linear regression against temperature (see details in Christian et al., 2001). Such model configuration may have a disadvantage for longer simulations and analyses, but has the advantage in reproducing the spatial patterns of most physical and biogeochemical fields.

The model is forced by atmospheric conditions: climatological monthly means of solar radiation and cloudiness, and interannual 6-day means of precipitation and surface wind stress. Precipitation is from ftp://ftp.cdc.noaa.gov/Datasets/gpcp. Wind stresses are from the National Centers for Environmental Prediction (NCEP) reanalysis (Kalnay et al., 1996). Air temperature and humidity above the ocean surface are computed by the atmospheric mixed layer model. Initial conditions

were obtained from outputs of an interannual hindcast simulation over 1948-2000, which itself is initialized from a 30-year spin up with climatological forcing, followed by two 40-year interannual simulations. The initial conditions for the spin up are specified from the WOA2013, iron concentration for the spin up was initialized from limited field data collected in the tropical Pacific (Johnson et al., 1997). We carry out an interannual simulation for the period of 1978-2010, and analyse the mean states from model simulations over the period of 1991-2010.

2.2 Ocean biogeochemical model

The DMEC model consists of eleven components: small (S) and large (L) sizes of phytoplankton (P_S and P_L), zooplankton (Z_S and Z_L) and detritus (D_S and D_L), dissolved organic nitrogen (DON), ammonium, nitrate, dissolved iron, and DO (Figure 1). Phytoplankton growth is co-limited by nitrogen and iron, which is critical in the tropical Pacific. The model simulates the iron cycle using variable Fe:N ratios, and incorporates atmospheric iron input. All biological components use nitrogen as their unit, in which sources/sinks are determined by biological and chemical processes in addition to the physical processes (circulation and vertical mixing) that are computed by the OGCM.

In this model, net community production (NCP) is computed as:

$$NCP = 6.625(\mu_s P_s + \mu_L P_L - r_s Z_s - r_L Z_L - c_{DON} DON - c_{DS} D_s - c_{DL} D_L) \quad (1)$$

where 6.625 is the C:N ratio, μ the rate constant of phytoplankton growth, r the rate constant of zooplankton respiration, c the rate constants of detritus decomposition and DON remineralization. The equations for biogeochemical processes and model parameters are given in Appendix A and B. There were changes in some parameters comparing with those in Wang et al. (2008), which were based on our model calibration and validation for chlorophyll (Wang et al., 2009a), nitrogen cycle (Wang et al., 2009b) and carbon cycle (Wang et al., 2015).

Recently, we have made further improvements in the parameterizations of detritus decomposition and DON remineralization (eq. B21-B23), which result from the first round of model calibration on DO distribution using WOA2013. In brief, c_{DON} decreases with depth over 100-1000 m, following an exponential function in this study. The differences in the related parameters are given in Appendix C.

2.3 Computation of oxygen sources and sinks

The time evolution of DO is regulated by physical, biological and chemical processes:

$$\frac{\partial O_2}{\partial t} = -u\frac{\partial O_2}{\partial x} - v\frac{\partial O_2}{\partial y} - w\frac{\partial O_2}{\partial z} + O_{mix} - O_{bio} + O_{gas} \quad (2)$$

where u, v, and w are zonal, meridional, and vertical velocity, respectively. O_{mix} is the vertical mixing term that is calculated by three subroutines. Briefly, the first one computes convection to remove instabilities in the water column, and the second

one determines the mixed layer depth. The third one computes partial vertical mixing (K_z) between two adjacent layers to relieve gradient Richardson (R_i) number instability, which is calculated as follows:

$$K_z = \left(1 - \left(\frac{Ri}{0.7}\right)^{\lambda}\right) (Ri < 0.7) \quad (3)$$

$$K_z = 0 \; (Ri \geq 0.7) \quad (4)$$

where the mixing parameter λ is set to 1. Clearly, partial vertical mixing is the dominant process influencing physical supply of DO in the intermediate waters.

The biological source/sink term O_{bio} is computed as follows:

$$O_{bio} = R_{OC}\mathrm{NCP} \quad (5)$$

where R_{OC} is the O:C utilization ratio (set to 1.3 in reference simulation, according to the Redfield ratio). Below the euphotic zone, DO concentration is determined by physical supply and biological consumption that results from detritus decomposition and DON remineralization, in which DON remineralization is dominant because DON pool is several times greater than detritus (Wang et al., 2008).

The flux of O_2 from the atmosphere to the surface ocean is computed as:

$$O_{gas} = (O_{Sat} - O)K_0 \quad (6)$$

where O_{sat} is the O_2 saturation, a function of temperature and salinity (Weiss, 1970), and K_0 the gas transfer velocity that is a function of wind speed (u_s) and SST according to Wanninkhof (1992):

$$K_0 = 0.31u_s^2\sqrt{\frac{S_c}{S_{c20}}} \quad (7)$$

where S_c and S_{c20} are the Schmidt number at SST and 20° C, respectively:

$$S_c = 1953 - 128T + 3.99T^2 - 0.05T^3 \quad (8)$$

3. Model experiments

3.1 Evaluation of DO distribution from the reference run

We first evaluate simulated DO for the tropical Pacific Ocean using the outputs from OGCM-DMEC V1.2 (hereafter reference run), which use the same set of parameters as Yu et al. (2021). We focus on model-data comparisons over 200-400 m, 400-700 m and 700-1000 m, that broadly represent the upper OMZ, lower OMZ and beneath OMZ, respectively. The WOA2013 data shows a much larger area of suboxic waters (<20 mmol m^{-3}) in the ETNP than in the ETSP over 200-400 m and 400-700 m (Figure 2a and 2c), but no suboxic water over 700-1000 m (Figure 2e). Although the reference run produces two OMZs off the equator over 200-400 m (Figure 2b), the sizes of suboxic water are much larger in the reference run than those in the WOA2013 data. The reference run significantly over-estimates the size of suboxic water and underestimates DO

concentration over 400-700 m (Figure 2d). The difference between WOA2013 and the reference run is small over 700-1000 m, except in the eastern tropical Pacific (Figure 2f).

3.2 Sensitivity experiments

There have been advances in understanding of oxygen consumption. For example, recent studies have showed that O:C utilization ratio varies largely across different basins, e.g., from 0.6 to 2.1 in the Pacific (Moreno et al., 2020; Tanioka and Matsumoto, 2020), and rates of DOM remineralization or oxygen consumption are influenced by oxygen level, i.e., a reduction under low DO conditions (Beman et al., 2020; Bertagnolli and Stewart, 2018; Sun et al., 2021). Based on the field data at mid-depth (~350 m) in the Peruvian OMZ (Kalvelage et al., 2015)， we derive a kinetics function between oxygen consumption rate and DO concentration, which yields the half saturation constant Km being 6.9 and 18.7 mmol m^{-3} (Figure 3). By adding this functional form to equation 5, one would get a varying and also reduced O:C utilization ratio, with lower ratios in in low-DO waters.

The reference run applied a zero value for background diffusion. However, a previous modelling study demonstrated that vertical background diffusion was an important process for DO supply at mid-depth (Duteil and Oschlies, 2011). Accordingly, we conduct a few more simulations (Table S1) to investigate how applying a reduced O:C utilization ratio (setting Km as 6.9 and 18.7 mmol m^{-3}) and adding background diffusion (setting Kb as 0.25 and 0.5 cm^2 s^{-1}) affect the simulated DO distribution and asymmetry of OMZs in the tropical Pacific. To eliminate complex interactions and feedbacks, the addition of background diffusion is only applied to the key variables (DO and DON) in this study.

Figure 4 illustrates that based on WOA2013 database, there is a larger volume of suboxic water located north of ~5°N and a smaller volume of suboxic water over 12°S-4°S, which are separated by relatively higher DO (>20 mmol m^{-3}) water along the equator. There is an improvement in simulated DO with reduced O:C utilization ratio (Figure 4b and 4c) and enhanced vertical mixing (Figure 4d and 4h). Clearly, combination of reduced O:C utilization ratio and enhanced vertical mixing leads to a further improvement in simulated mid-depth DO (Figure 4e, 4f, 4i and 4j). In particular, the combination of a stronger background diffusion with a smaller O:C utilization ratio (i.e., the Km18.7Kb0.5 run) results in the best simulation that reproduces the observed spatial distribution of mid-depth DO, especially the asymmetric feature (i.e., a larger volume of suboxic water to the north but a smaller size of suboxic water to the south).

3.3 Model validation

To further evaluate the performance of experiments, a few statistical measures are applied over 200-400 m, 400-700 m and 700-1000 m in the ETNP (165°W-90°W, 5°-20°N) and ETSP (110°W-80°W, 10°S-3°S). As shown in Table 1, compared with the reference run, bias and root mean square error (RMSE) are reduced in all new simulations, with the smallest values from Km18.7Kb0.5 run except over 700-1000 m in the ETNP. For example, both bias and RMSE in the Km18.7Kb0.5 run

are smallest over 200-700 m in the ETNP (<7.8 and 10.2 mmol m^{-3}). Many current models show much large RMSE (~20-80 mmol m^{-3}) with respect to observed DO from mixed layer to 1000 m (Bao and Li, 2016; Cabre et al., 2015). Figure 5 also illustrates that the Km18.7Kb0.5 run produces the best outputs, with the largest correlation coefficients (0.77-0.94) and also the smallest distance to 1 in normalized standard deviation (0.54-1.81 in ETNP and 0.33-1.63 in ETSP).

We also compare the sizes of suboxic water and hypoxic water between model simulations and WOA2013 (Table 2). Based on WOA2013, sizes of suboxic water and hypoxic water are $5.97x10^{15}$ m^3 and $19.98x10^{15}$ m^3 in the north, and 1.43×10^{15} m^3 and $7.12x10^{15}$ m^3 in the south, respectively. While reduced O:C utilization ratio and enhanced vertical mixing can lead to an improvement in simulated OMZ volume, a significant improvement is obtained with the combination of reduced O:C utilization ratio and enhanced vertical mixing. Overall, the Km18.7Kb0.5 simulation has the best performance for reproducing the OMZ volumes, showing similar volumes for the suboxic water ($5.55x10^{15}$ m^3 to the north and $1.12x10^{15}$ m^3 to the south) and the hypoxic water ($20.91x10^{15}$ m^3 and $7.39x10^{15}$ m^3).

We then further validate the modelled DO from the best run (Km18.7Kb0.5), using the time series of the observed DO data (https://cchdo.ucsd.edu/). Figure 6 illustrates that the model can generally reproduce the vertical-zonal distributions of DO along 10°N and 17°S, spanning from 1989 to 2009, particularly in the eastern tropical Pacific. For example, cruise data from the P04 line during April-May, 1989 show a large area of low DO water spanning from ~200 m to ~800 m (Figure 6a), and our model also predicts low DO water over ~200-700 m (Figure 6b).

4 Model results and discussions

In this section, we further compare the improved model simulations (Km18.7, Kb0.5 and Km18.7Kb0.5) with the reference run to diagnose the influences of improved parameterizations on the distribution of mid-depth DO, and biological consumption and physical supply. We then analyse the interactions of physical and biogeochemical processes, and the impacts on the source and sink for the mid-depth DO. In the end, we explore the underlying mechanisms regulating the asymmetry of OMZs in the tropical Pacific.

4.1 Changes of mid-depth DO due to reduced O:C utilization ratio and enhanced vertical mixing

We first compare the changes in DO concentrations between the three model simulations over 200-400 m, 400-700 m, and 700-1000 m (Figure 7). Clearly, applying a reduced O:C utilization ratio causes an increase of DO in all three layers, with the greatest increase (>6 mmol m^{-3}) in the 200-400 m layer (Figure 7a), followed by a modest increase (~3-6 mmol m^{-3}) over 400-700 m (Figure 7d). Although DO increase is generally smaller in the 700-1000 m layer (Figure 7h) than in the 400-700 m layer (Figure 7d), the increase is greater in the north OMZ over 700-1000 m than over 400-700 m. Enhanced vertical

mixing results in a small increase of DO (~2-5 mmol m^{-3}) in the 10°S-10°N band over 200-400 m (Figure 7b), but a large increase (~5-15 mmol m^{-3}) in majority of the basin over 400-700 m and 700-1000 m (Figure 7e and 7i).

Overall, the mid-depth DO shows an increase with the combination of a reduced O:C utilization ratio and enhanced vertical mixing (Figure 7c, 7f & 7j). A great increase of DO (>15 mmol m^{-3}) occurs in majority of the basin over 400-700 m, mainly in the central tropical Pacific over 200-400 m, but in a few small areas over 700-1000 m. The spatial pattern and magnitude of DO increase resulting from the combination of reduced O:C utilization ratio and enhanced vertical mixing, have a large similarity to those with reduced O:C utilization ratio for the 200-400 m layer (Figure 7a), but to those under enhanced vertical mixing below 400 m (Figure 7e & 7i). For example, the relative increase of DO is similarly larger in the northern OMZ over 200-400 m under a reduced O:C utilization ratio with and without the addition of background diffusion, and over 700-1000 m under enhanced vertical mixing (i.e., with additional background diffusion) with and without the change in the O:C utilization ratio. Our analyses suggest that the dominant process regulating the DO dynamics is biological consumption over 200-700 m, but physical supply over 400-1000 m.

4.2 Effects of reduced O:C utilization ratio and enhanced vertical mixing on consumption and supply

To better understand the effects of changes in the biological and/or physical parameters on the DO dynamics, we then evaluate the responses of biological consumption and physical supply. As illustrated in Figure 8, changes in biological consumption are almost identical under a reduced O:C utilization ratio with or without background diffusion. In particular, biological consumption shows a large decrease (~2-8 mmol m^{-3} yr^{-1}) over 200-400 m (Figure 8b), and a small decrease (~0.2-1.0 mmol m^{-3} yr^{-1}) over 400-700 m, with the largest decrease in the northern OMZ (Figure 8e); there is a very small change in biological consumption over 700-1000 m, i.e., a decrease of <0.1 mmol m^{-3} yr^{-1} over majority of the basin but an increase of <0.1 mmol m^{-3} yr^{-1} in some parts of subtropical region (Figure 8i). On the other hand, enhanced vertical mixing leads to a small increase (<0.2 mmol m^{-3} yr^{-1}) in biological consumption in all three layers, with a relatively larger increase in the northern OMZ (Figure 8c, 8f and 8j).

Figure 9 shows the effects of a reduced O:C utilization ratio and enhanced vertical mixing on physical supply. With the combination of a reduced O:C utilization ratio and enhanced vertical mixing, physical supply shows a small increase (by ~0.2-1.0 mmol m^{-3} yr^{-1}) in the whole basin over 700-1000 m (Figure 9h) and only outside the OMZs over 400-700 m (Figure 9d), but a relatively larger decrease in the OMZs over 200-700 m (by ~0.2-6 mmol m^{-3} yr^{-1}) (Figure 9a and 9d). Clearly, enhanced vertical mixing leads to an increase of physical supply over majority of the basin, with greater increase over 400-1000 m (~0.2-1.0 mmol m^{-3} yr^{-1}) than over 200-400 m (~0-0.4 mmol m^{-3} yr^{-1}) (Figure 9c, 9f and 9j). However, applying a reduced O:C utilization ratio causes a large decrease of physical supply above 700 m, with greater decrease over 400-700 m in the OMZs (~0.2-6 mmol m^{-3} yr^{-1}), and very small changes (<0.2 mmol m^{-3} yr^{-1}) over 700-1000 m (Figure 9b, 9e and 9i). Overall, rate of physical supply is largely determined by vertical mixing over 700-1000 m, by both vertical mixing and

biological consumption over 400-700 m, but by consumption over 200-400 m, implying complex physical-biological interactions and feedbacks in the tropical Pacific OMZs.

4.3 Interactive effects of physical and biological processes on source and sink of mid-depth DO

There is evidence that enhanced mixing can have large influences not only on physical processes (e.g., the strength of water mixing) but also on biological processes (e.g., transport of organic materials), which have direct or indirect effects on the evolution of mid-depth DO (Andrews et al., 2017; Duteil and Oschlies, 2011; Stramma et al., 2012). Our analyses show an increase in physical supply under enhanced vertical mixing in most parts of the 200-1000 m layer in the eastern tropical Pacific (over 120°W-90°W) (Figure 10). Interestingly, the greater increase (>1 mmol m^{-3} yr^{-1}) is below the OMZs over 15°S-10°N using 1.3 as the O:C utilization ratio (Figure 10a), but occurs over a much larger area (i.e., over 15°S-20°N) and within the OMZs using a reduced (and also varying) O:C utilization ratio (Figure 10d). Enhanced vertical mixing also results in a generally small increase in biological consumption, with greater increases in OMZs using a reduced O:C utilization ratio (Figure 10e) than using a constant Redfield ratio of 1.3 (Figure 10b). The small increase in consumption outside of OMZs is largely attributable to increased DON concentration (data not shown) that results from the enhanced vertical mixing whereas the increase of consumption inside the OMZs would be a result of the interactions and feedbacks of various physical, biological and chemical processes. Clearly, there is an overall increase in net flux, with the largest increases occurring mainly outside the OMZs (Figure 10c and 10f).

To further investigate the interactive effects of a reduced O:C utilization ratio and enhanced mixing, we then compare the responses of biological consumption and physical supply to changes in the O:C utilization ratio with and without background diffusion (Figure 11). While a reduced O:C utilization ratio can result in a decrease in consumption above 600 m, the decrease is slightly less in the OMZs with background diffusion (Figure 11d) than without background diffusion (Figure 11a). Similarly, physical supply also shows a decrease in the OMZs under a reduced O:C utilization ratio (Figure 11b), with a lesser decrease under the addition of background diffusion (Figure 11e). The greatest difference is found in the core OMZs for both biological consumption (Figure 11h) and physical supply (Figure 11i), but larger differences are found in supply. A previous modeling study also demonstrates that physical contribution to the changes of DO is much greater than biogeochemical contribution (Montes et al., 2014). However, a reduced O:C utilization ratio results in a clear increase in net flux in the whole water column over 200-1000 m, with a great increase above the core OMZs within the 10°S-10°N band (Figure 11c and 11f).

Physical supply could be divided into horizontal advection, vertical advection, and vertical mixing. Our model performs well in simulating the meridional and zonal advections, and vertical mixing processes of DO transport (see Figure S2), which allows us to evaluate the responses of different supply components to the reduced O:C utilization ratio. As shown in Figure 12, there is no clear pattern in the responses of advective supply, with very small values (< ~1 mmol m^{-3} yr^{-1}) over the entire

basin (Figure 12h and 12i). However, the DO supply by vertical mixing shows a strong response, with similar patterns to those of total supply and a large decrease in the suboxic waters (Figure 12c and 12f). While applying a reduced O:C utilization ratio causes a decrease in the DO supply (~1-6 mmol m^{-3} yr^{-1}) by vertical mixing, the decrease is larger in the OMZs without the addition of background diffusion. On the other hand, there is an increase in the supply by vertical mixing below the OMZs under a reduced O:C utilization ratio, in particular with the addition of background diffusion (Figure 12f). The largest difference (~1-2 mmol m^{-3} yr^{-1}) is found within the hypoxic waters (Figure 12j), which reflects the strong feedback between physical and biological processes in the OMZs.

There is evidence that the physical and biogeochemical processes have multiple interactions with impacts on various physical, chemical and biological fields and implications for DO dynamics (Breitburg et al., 2018; Duteil and Oschlies, 2011; Oschlies et al., 2018). For example, observational and modelling studies show that changes in vertical mixing intensity can affect the distributions of organic matter thus oxygen consumption at mid-depth (Duteil and Oschlies, 2011; Talley et al., 2016), and vertical distributions of DOM concentration and its remineralization around the OMZ in turn can alter the intensity of vertical mixing for DO (Loginova et al., 2019). Recent studies have demonstrated that a changing O:C utilization ratio (or respiration quotient) has various impacts on biological and chemical processes, with an impact on microbial respiration thus oxygen consumption (Moreno et al., 2020; Tanioka and Matsumoto, 2020). In particular, applying a smaller O:C utilization ratio leads to lower consumption rates, thus higher DO levels (Moreno et al., 2020), which would have large effects on DO gradients thus vertical mixing particularly in low-DO waters (e.g., in the OMZs).

4.4 Impacts of biological and physical processes on asymmetric OMZs

There is evidence of asymmetric features in many biogeochemical parameters in the tropical Pacific. For example, POC flux at 500 m is greater in the northern tropical Pacific (~4 mmol C m^{-2} d^{-1}) (Van Mooy et al., 2002) than in the southern tropical Pacific (<1 mmol C m^{-2} d^{-1}) (Pavia et al., 2019). Similarly, our regional model reproduces an asymmetric pattern for POC flux, with larger values to the north than to the south. Field studies have reported an asymmetry in DOM distribution over ~200-1000 m in the central-eastern tropical Pacific, i.e., higher levels of DON and DOC to the north than to the south (Hansell, 2013; Libby and Wheeler, 1997; Raimbault et al., 1999). Our model simulation also reveals an asymmetric DON at mid-depth, i.e., ~6-7 mmol m^{-3} in the ETNP and ~4-5 mmol m^{-3} in the ETSP (data not show). However, an earlier field study reported higher rates of organic carbon remineralization over 200-1000 m to the south (~2-10 mmol m^{-3} yr^{-1}) than to the north (~1-6 mmol m^{-3} yr^{-1}) in the eastern/central tropical Pacific (Feely et al., 2004). Similarly, our model simulation also shows such asymmetric feature of biological consumption below 200 m in the tropical Pacific, i.e., ~2-8 mmol m^{-3} yr^{-1} in the ETSP and ~1-6 mmol m^{-3} yr^{-1} in the ETNP.

It appears that the asymmetric distributions differ largely between biological parameters, and there are almost opposite patterns between oxygen consumption (or DOM remineralization) and DOM concentration. This discrepancy may be

attributed to the rates of DOM remineralization in the water column, which is determined not only by DOM concentration, but also by the stoichiometry associated with microbial respiration (Wang et al., 2008; Zakem and Levine, 2019). Recent studies on respiration quotient demonstrate that the O:C utilization ratio is lower to the north than to the south in the tropical Pacific (Tanioka and Matsumoto, 2020; Wang et al., 2019), which primarily reflects the difference in oxygen limitation on microbial respiration (Kalvelage et al., 2015). Apparently, such asymmetry in biological consumption cannot explain the asymmetry in the tropical Pacific OMZs (i.e., lower DO levels to the north than to the south), indicating that other processes are responsible for the asymmetry.

Numerous studies have indicated that physical mixing is the only source of DO for the tropical OMZs (Brandt et al., 2015; Czeschel et al., 2012; Duteil et al., 2020). For example, turbulent diffusion is argued to account for 89% of the net DO supply for the core OMZ of south tropical Pacific (Llanillo et al., 2018). There is evidence that larger-scale mass transport due to circulation and ventilation is more efficient in the south Pacific than in the north Pacific (Kuntz and Schrag, 2018), and the transit time from the surface to the OMZ is much longer in the ETNP than in the ETSP (Fu et al., 2018). Both our analyses and other modeling studies (Duteil, 2019; Shigemitsu et al., 2017) demonstrate that DO supply via vertical mixing is much weaker in the northern OMZ than in the southern OMZ in the tropical Pacific. All these analyses indicate that physical processes play a major role in shaping the asymmetry of the OMZs over the tropical Pacific.

4.5 Implications and limitations of the current research

There are inter-dependencies between the physical and biogeochemical processes (Duteil and Oschlies, 2011; Gnanadesikan et al., 2012; Niemeyer et al., 2019), which may have influences on the asymmetry of OMZs in the tropical Pacific. Our study shows that rate of physical supply is sensitive to changes in both physical and biological parameterizations, particularly in low-DO waters. Since the physical contribution exceeds the biological contribution to mid-depth DO in the tropical Pacific (Llanillo et al., 2018; Montes et al., 2014), and the physical processes are more dominant in the ETSP, one may expect that physical-biological feedbacks are stronger to the south, which can lead to relatively larger net flux into the south OMZ.

Physical and biogeochemical interactions are complex over space, which have direct and indirect effects on the source and sink of DO (Levin, 2018; Oschlies et al., 2018). On the one hand, supply of DO is greater under stronger physical transport in the south tropical Pacific. On the other hand, stronger physical processes can also lead to higher levels of nutrients and biological production and thus enhanced export production and oxygen consumption at mid-depth (Duteil and Oschlies, 2011), which can offset the rate of physical supply. In addition, stronger physical processes can also result in strengthened transport of DO and OM out to other regions (Gnanadesikan et al., 2012; Yu et al., 2021), which has complex impacts on DO balance in the southern OMZ.

There is evidence of strong interactions and feedbacks between carbon, nitrogen and oxygen cycles in marine ecosystem. Limited studies indicate that O:C:N utilization ratios during microbial respiration vary largely in the water column (Moreno et al., 2020; Zakem and Levine, 2019), and nitrogen cycling (e.g., oxidation, nitrification and denitrification) not only has impacts on oxygen consumption/production but also is influenced by the oxygen level (Beman et al., 2021; Kalvelage et al., 2013; Oschlies et al., 2019; Sun et al., 2021). However, little attention has been paid to understand the coupling of carbon and oxygen cycles. It should be noted that the available data are also not sufficient for the parameterizations of relevant processes, which has hampered our ability to assess the impacts of biogeochemical processes associated with the nitrogen cycle on oxygen fields. Future observational and modelling studies are needed not only to improve our knowledge on the coupling of carbon, nitrogen and oxygen cycles in the ocean, but also to advance our understanding on the physical and biogeochemical interactions and feedbacks associated with the marine stoichiometry.

5. Conclusion

In this paper, we use a basin scale model to investigate the impacts of parameterizations of vertical mixing and DOM remineralization on the dynamics of mid-depth DO, and analyse the underlying mechanisms for asymmetric OMZs in the tropical Pacific. Our study shows that the model is capable of reproducing the observed DO distributions and asymmetric OMZs with the combination of enhanced vertical mixing and reduced O:C utilization ratio that causes an increase in DO concentration (or net flux) at mid-depth. Overall, enhanced vertical mixing makes a greater contribution to the increase over 400-1000 m, and the contribution from reduced O:C utilization ratio is greater over 200-700 m.

Our analyses demonstrate that there is a large increase in physical supply and a small increase in biological consumption under enhanced vertical mixing, and the increase in consumption is a result of redistribution of DOM in the water column. On the other hand, applying a reduced O:C utilization ratio leads to a large decrease in biological consumption, and a small decrease in physical supply (due to the vertical changes in DO gradients). These findings point to strong physical-biological interactions and feedbacks in the tropical Pacific OMZs.

This study suggest that biological consumption (i.e., greater rate to the south) cannot explain the asymmetric feature in the tropical Pacific OMZs (i.e., lower DO levels to the north), but physical processes (i.e., stronger supply to the south) play a major role in shaping the asymmetric OMZs of the tropical Pacific. In addition, the interactions between physical and biological processes are also stronger in the southern OMZ than in the northern OMZ, probably because physical supply is sensitive to changes in both parameterizations of vertical mixing and DOM remineralization. Further studies with improved approaches will enable to better understand the interactions and feedbacks between physical and biogeochemical processes.

Appendix A: Model biogeochemical equations

Phytoplankton equations

$$\frac{\partial P_S}{\partial t} = \mu_S P_S - g_{P_S}(1 - e^{-\Lambda P_S})Z_S - m_S P_S \quad \text{(B1)}$$

$$\frac{\partial P_L}{\partial t} = \mu_L P_L - g_{P_L1}(1 - e^{-\Lambda P_L})Z_L - g_{P_L2}(1 - e^{-\Lambda P_L})Z_S - m_L P_L \quad \text{(B2)}$$

Zooplankton equations

$$\frac{\partial Z_S}{\partial t} = [\lambda(g_{P_S}(1 - e^{-\Lambda P_S}) + g_{P_L2}(1 - e^{-\Lambda P_L})) + g_{D_S}(1 - e^{-\Lambda D_S}) + g_{D_L2}(1 - e^{-\Lambda D_L}) - (r_s + \delta_s)]Z_S - g_{Z_S}(1 - e^{-\Lambda Z_S})\, Z_L \quad \text{(B3)}$$

$$\frac{\partial Z_L}{\partial t} = [\lambda(g_{P_L1}(1 - e^{-\Lambda P_L}) + g_{Z_S}(1 - e^{-\Lambda Z_S})) + g_{D_L1}(1 - e^{-\Lambda D_L}) - (r_L + \delta_L)]Z_L \quad \text{(B4)}$$

Detritus equations

$$\frac{\partial D_S}{\partial t} = (m_S P_S + m_L P_L + (r_s Z_S + r_L Z_L)\chi)(1 - \gamma) - g_{D_S}(1 - e^{-\Lambda D_S})Z_S - (c_{D_S} + \omega_{D_S} h^{-1})D_s \quad \text{(B5)}$$

$$\frac{\partial D_L}{\partial t} = (1 - \lambda)[\left(g_{P_S}(1 - e^{-\Lambda P_S}) + g_{P_L2}(1 - e^{-\Lambda P_L})\right)Z_S + \left(g_{P_L1}(1 - e^{-\Lambda P_L}) + g_{Z_S}(1 - e^{-\Lambda Z_S})\right)Z_L] + \delta_S Z_S + \delta_L Z_L - (c_{D_L} + \omega_{DL} h^{-1})D_L - g_{D_L2}(1 - e^{-\Lambda D_L})Z_S - g_{D_L1}(1 - e^{-\Lambda D_L})Z_L \quad \text{(B6)}$$

DON equations

$$\frac{\partial DON}{\partial t} = (m_S P_S + m_L P_L + (r_s Z_S + r_L Z_L)\chi)\gamma + (c_{D_S} D_S + c_{D_L} D_L)\zeta - c_{DON} DON \quad \text{(B7)}$$

Nutrients equations

$$\frac{\partial \mathrm{NO_3}}{\partial t} = -\mu_S P_S \frac{N_{S\_UP}}{N_{S\_UP} + A_{UP}} - \mu_L P_L \frac{N_{L\_UP}}{N_{L\_UP} + A_{UP}} + \varphi NH_4 \quad \text{(B8)}$$

$$\frac{\partial \mathrm{NH_4}}{\partial t} = -\mu_S P_S \frac{A_{up}}{N_{S\_UP} + A_{UP}} - \mu_L P_L \frac{A_{up}}{N_{L\_UP} + A_{UP}} + (r_S Z_S + r_L Z_L)(1 - \chi) + c_{DON} DON + (c_{D_S} D_S + c_{D_L} D_L)(1 - \zeta) - \varphi NH_4 \quad \text{(B9)}$$

$$\frac{\partial \mathrm{Fe}}{\partial t} = -(\mu_S P_S R_S + \mu_L P_L R_L - s_{Fe} D_L Fe) + R_S[(r_S Z_S + r_L Z_L)(1 - \chi) + c_{DON} DON + c_{D_S} D_S + c_{D_L} D_L(1 - \zeta)] \quad \text{(B10)}$$

Nitrogen uptake

$$N_{S\_UP} = \frac{NO_3}{K_{S\_NO_3} + NO_3}\left(1 - \frac{NH_4}{K_{NH_4} + NH_4}\right) \quad \text{(B11)}$$

$$N_{L\_UP} = \frac{NO_3}{K_{L\_NO_3} + NO_3}\left(1 - \frac{NH_4}{K_{NH_4} + NH_4}\right) \quad \text{(B12)}$$

$$A_{UP} = \frac{NH_4}{K_{NH_4}+NH_4} \quad \text{(B13)}$$

Other equations

Phytoplankton growth rate

$$\mu_S = \mu_{S0} e^{k_T T} f(I) \psi_S(N, Fe) \quad \text{(B14)}$$

$$\mu_L = \mu_{L0} e^{k_T T} f(I) \psi_L(N, Fe) \quad \text{(B15)}$$

Nutrient limitation

$$\psi_S(N, Fe) = \min\left(\frac{NO_3+NH_4}{K_{S\_N}+NO_3+NH_4}, \frac{\mathrm{Fe}}{K_{S\_\mathrm{Fe}}+\mathrm{Fe}}\right) \quad \text{(B16)}$$

$$\psi_L(N, Fe) = \min\left(\frac{NO_3+NH_4}{K_{L\_N}+NO_3+NH_4}, \frac{\mathrm{Fe}}{K_{L\_\mathrm{Fe}}+\mathrm{Fe}}\right) \quad \text{(B17)}$$

Light limitation

$$f(I) = 1 - e^{-\frac{\alpha I}{\eta P_{MAX}}} \quad \text{(B18)}$$

Light attenuation

$$I(z) = I_0 exp^{-k_A Z} \quad \text{(B19)}$$

$$k_A = k_W + k_C \mathrm{Chl} + k_D(D_S+D_L) \quad \text{(B20)}$$

Detritus decomposition and DON remineralization

$$c_{DS} = c_{DS0} e^{k_B(T-T_0)} \quad \text{(B21)}$$

$$c_{DL} = c_{DL0} e^{k_B(T-T_0)} \quad \text{(B22)}$$

$$c_{DON} = c_{DON0} e^{k_B(T-T_0)} \quad \text{(B23)}$$

Phytoplankton carbon to chlorophyll ratio (η)

$$\mathrm{Chl} = \left(\frac{P_S}{\eta_S} + \frac{P_L}{\eta_L}\right) R_{C:N} \quad \text{(B24)}$$

$$\eta_S = \eta_{S0} - (\eta_{S0} - \eta_{MIN}) \frac{lnI_0 - lnI}{4.605} \quad \text{(B25)}$$

$$\eta_L = \eta_{L0} - (\eta_{L0} - \eta_{MIN}) \frac{lnI_0 - lnI}{4.605} \quad \text{(B26)}$$

$$\eta_{S0} = \eta_{S\_MAX} - k_{PS} \mu_S^* \quad \text{(B27)}$$

$$\eta_{L0} = \eta_{L\_MAX} - k_{PL} \mu_L^* \quad \text{(B28)}$$

$$\mu_S^* = \mu_{S0} e^{k_T T} \min\left(\frac{NO_3}{K_{S\_N}+NO_3}, \frac{\mathrm{Fe}}{K_{S\_\mathrm{Fe}}+\mathrm{Fe}}\right) \quad \text{(B29)}$$

$$\mu_L^* = \mu_{L0} e^{k_T T} \min\left(\frac{NO_3}{K_{L\_N}+NO_3}, \frac{\mathrm{Fe}}{K_{L\_\mathrm{Fe}}+\mathrm{Fe}}\right) \quad \text{(B30)}$$

Appendix B: Model biogeochemical parameters

Symbol	Parameter	Unit	Value
m_S	Small phytoplankton mortality rate	d^{-1}	0.15
m_L	Large phytoplankton mortality rate	d^{-1}	0.35
r_S	Small zooplankton excretion rate	d^{-1}	0.53
r_L	Large zooplankton excretion rate	d^{-1}	0.44
δ_S	Small zootoplankton mortality rate	d^{-1}	0.12
δ_L	Large zootoplankton mortality rate	d^{-1}	0.12
g_{PS}	Maximum grazing rate for small phytoplanktion	d^{-1}	2.6
g_{PL1}	Maximum grazing rate for large phytoplanktion	d^{-1}	1.2
g_{ZS}	Maximum grazing rate for small zootoplanktion	d^{-1}	1.7
g_{PL2}	Maximum grazing rate for large phytoplanktion	d^{-1}	0.9
g_{DS}	Maximum grazing rate for small detritus	d^{-1}	1.0
g_{DL1}	Maximum grazing rate for large detritus	d^{-1}	3.0
g_{DL2}	Maximum grazing rate for large detritus	d^{-1}	1.5
Λ	Ivlev coefficient	$(mmol\ m^{-3})^{-1}$	0.5
λ	Zootoplankton assimilation coefficient	%	75
χ	Excretion coefficient	%	55
γ	Dissolution coefficient	%	90
ξ	Dissolution coefficient	%	90
$R_{C:N}$	C:N ratio	mol:mol	6.625
R_S	Fe:N ratio for small phytoplankton	μmol:mol	15
R_L	Fe:N ratio for large phytoplankton	μmol:mol	40
η_{S_MIN}	Minimum PhyC:Chl ratio in small phytoplanktion	g:g	30
η_{L_MIN}	Minimum PhyC:Chl ratio in large phytoplanktion	g:g	15
η_{S_MAX}	Maximum PhyC:Chl ratio in small phytoplanktion	g:g	200
η_{L_MAX}	Maximum PhyC:Chl ratio in large phytoplanktion	g:g	120
k_{PS}	Photoacclimation coefficient for small phytoplanktion	(g:g)d	95
k_{PL}	Photoacclimation coefficient for large phytoplanktion	(g:g)d	70

w_{DS}	Sinking velocity for small detritus	m d^{-1}	1
w_{DL}	Sinking velocity for large detritus	m d^{-1}	3.5
φ	Nitrification rate (when I<5 μmolEm^{-2} s^{-1})	d^{-1}	0.04
s_{Fe}	Iron scavenge coefficient	d^{-1} (nmol Fe m^{-3})$^{-1}$	0.00001
μ_{S0}	Maximum growth rate at 0°C for small phytoplankton	d^{-1}	0.58
μ_{L0}	Maximum growth rate at 0°C for large phytoplankton	d^{-1}	1.16
k_T	Temp. Dependent coefficient for μ	$°C^{-1}$	0.06
K_{S_N}	Half saturation constant for N limitation	mmol m^{-3}	0.3
K_{L_N}	Half saturation constant for N limitation	mmol m^{-3}	0.9
K_{S_Fe}	Half saturation constant for iron limitation	mmol m^{-3}	14
K_{L_Fe}	Half saturation constant for iron limitation	mmol m^{-3}	150
K_{S_NO3}	Half saturation constant for nitrate uptake	mmol m^{-3}	0.3
K_{L_NO3}	Half saturation constant for nitrate uptake	mmol m^{-3}	0.9
K_{NH4}	Half saturation constant for ammonium uptake	mmol m^{-3}	0.05
α	Initial slope of the P – I curve	mg C mg chl^{-1}(μmol E m^{-2} s^{-1})$^{-1}$	0.02
P_{MAX}	Maximum carbon specific growth rate	h^{-1}	0.036
k_W	Light attenuation constant for water	m^{-1}	0.028
k_C	Light attenuation constant for chlorophyll	m^{-1} (mg chl m^{-3})$^{-1}$	0.058
k_D	Light attenuation constant for detritus	m^{-1} (mg chl m^{-3})$^{-1}$	0.008
c_{DS0}	Small detritus decomposition rate at 0°C	d^{-1}	0.001
c_{DL0}	Large detritus decomposition rate at 0°C	d^{-1}	0.008

445

Appendix C: Comparisons in biogeochemical parameters

Symbol	Parameter	Unit	Yu et al. (2021)	This study
T_0	Limit temperature	℃	10	0
k_B	Temperature dependent coefficient	-	0.002	0.001
C_{DON0}	DON remineralization constant	d^{-1}		
	0-100 m		0.001	0.00075
	100-600 m		0.0002-0.001	0.00013-0.00075*
	600-1000 m		0.0002	0.00003-0.00013*

* C_{DON0} decreases with depth by an exponential function.

Code and data availability. The exact version of the software code used to produce the results presented in this paper is archived on Zenodo (https://doi.org/10.5281/zenodo.5148146, Wang et al., 2021). Other code and data are available upon request from the authors. Request for materials should be addressed to X.J.W. (xwang@bnu.edu.cn).

Author contributions. X.J.W. and K.W. designed the study, performed the simulations and prepared the manuscript. R.M., D.X.Z. and R.H.Z. contributed to analysis, interpretation of results and writing.

Competing interests. The authors declare that they have no conflict of interest.

Acknowledgements. This work was supported by the Chinese Academy of Sciences' Strategic Priority Project (XDA1101010504). The authors wish to acknowledge the use of the Ferret (http://ferret.pmel.noaa.gov/Ferret/).

References

Andrews, O., Buitenhuis, E., Le Quere, C., and Suntharalingam, P.: Biogeochemical modelling of dissolved oxygen in a changing ocean, Philosophical transactions. Series A, Mathematical, physical, and engineering sciences, 375, 2017.

Bao, Y. and Li, Y.: Simulations of dissolved oxygen concentration in CMIP5 Earth system models, Acta Oceanologica Sinica, 35, 28-37, 2016.

Beman, J. M., Vargas, S. M., Vazquez, S., Wilson, J. M., Yu, A., Cairo, A., and Perez-Coronel, E.: Biogeochemistry and hydrography shape microbial community assembly and activity in the eastern tropical North Pacific Ocean oxygen minimum zone, Environmental microbiology, 23, 2765-2781, 2021.

Beman, J. M., Vargas, S. M., Vazquez, S., Wilson, J. M., Yu, A., Cairo, A., and Perez-Coronel, E.: Biogeochemistry and hydrography shape microbial community assembly and activity in the eastern tropical North Pacific Ocean oxygen minimum zone, Environmental microbiology, 23, 2765-2781, 2020.

Bertagnolli, A. D. and Stewart, F. J.: Microbial niches in marine oxygen minimum zones, Nature reviews. Microbiology, 16, 723-729, 2018.

Berthet, S., Séférian, R., Bricaud, C., Chevallier, M., Voldoire, A., and Ethé, C.: Evaluation of an Online Grid‐Coarsening Algorithm in a Global Eddy‐Admitting Ocean Biogeochemical Model, Journal of Advances in Modeling Earth Systems, 11, 1759-1783, 2019.

Bettencourt, J. H., Lopez, C., Hernandez-Garcia, E., Montes, I., Sudre, J., Dewitte, B., Paulmier, A., and Garcon, V.: Boundaries of the Peruvian oxygen minimum zone shaped by coherent mesoscale dynamics, Nature Geoscience, 8, 937-U967, 2015.

Bianchi, D., Dunne, J. P., Sarmiento, J. L., and Galbraith, E. D.: Data-based estimates of suboxia, denitrification, and N2O production in the ocean and their sensitivities to dissolved O2, Global Biogeochemical Cycles, 26, 1-13, 2012.

Bopp, L., Le Quere, C., Heimann, M., Manning, A. C., and Monfray, P.: Climate-induced oceanic oxygen fluxes: Implications for the contemporary carbon budget, Global Biogeochemical Cycles, 16, 1-13, 2002.

Brandt, P., Bange, H. W., Banyte, D., Dengler, M., Didwischus, S. H., Fischer, T., Greatbatch, R. J., Hahn, J., Kanzow, T., Karstensen, J., Krortzinger, A., Krahmann, G., Schmidtko, S., Stramma, L., Tanhua, T., and Visbeck, M.: On the role of circulation and mixing in the ventilation of oxygen minimum zones with a focus on the eastern tropical North Atlantic, Biogeosciences, 12, 489-512, 2015.

Breitburg, D., Levin, L. A., Oschlies, A., Gregoire, M., Chavez, F. P., Conley, D. J., Garcon, V., Gilbert, D., Gutierrez, D., Isensee, K., Jacinto, G. S., Limburg, K. E., Montes, I., Naqvi, S. W. A., Pitcher, G. C., Rabalais, N. N., Roman, M. R., Rose, K. A., Seibel, B. A., Telszewski, M., Yasuhara, M., and Zhang, J.: Declining oxygen in the global ocean and coastal waters, Science, 359, 2018.

Busecke, J. J. M., Resplandy, L., and Dunne, J. P. P.: The Equatorial Undercurrent and the Oxygen Minimum Zone in the Pacific, Geophysical Research Letters, doi: 10.1029/2019GL082692, 2019. 6716–6725, 2019.

Cabre, A., Marinov, I., Bernardello, R., and Bianchi, D.: Oxygen minimum zones in the tropical Pacific across CMIP5 models: mean state differences and climate change trends, Biogeosciences, 12, 5429-5454, 2015.

Chen, D., Rothstein, L. M., and Busalacchi, A. J.: A Hybrid Vertical Mixing Scheme and Its Application to Tropical Ocean Models, Journal of Physical Oceanography, 24, 2156-2179, 1994.

Christian, J. R., Verschell, M. A., Murtugudde, R., Busalacchi, A. J., and McClain, C. R.: Biogeochemical modelling of the tropical Pacific Ocean. I: Seasonal and interannual variability, Deep Sea Research Part II: Topical Studies in Oceanography, 49, 509-543, 2001.

Czeschel, R., Stramma, L., and Johnson, G. C.: Oxygen decreases and variability in the eastern equatorial Pacific, J Geophys Res-Oceans, 117, 1-12, 2012.

Czeschel, R., Stramma, L., Schwarzkopf, F. U., Giese, B. S., Funk, A., and Karstensen, J.: Middepth circulation of the eastern tropical South Pacific and its link to the oxygen minimum zone, J Geophys Res-Oceans, 116, 2011.

Duteil, O.: Wind Synoptic Activity Increases Oxygen Levels in the Tropical Pacific Ocean, Geophysical Research Letters, 46, 2715-2725, 2019.

Duteil, O., Frenger, I., and Getzlaff, J.: Intermediate water masses, a major supplier of oxygen for the eastern tropical Pacific ocean, Ocean Science, doi: 10.5194/os-2020-17, 2020. 2020.

Duteil, O. and Oschlies, A.: Sensitivity of simulated extent and future evolution of marine suboxia to mixing intensity, Geophysical Research Letters, 38, 2011.
Feely, R. A., Sabine, C. L., Schlitzer, R., Bullister, J. L., Mecking, S., and Greeley, D.: Oxygen utilization and organic carbon remineralization in the upper water column of the Pacific Ocean, Journal of Oceanography, 60, 45-52, 2004.
Fu, W. W., Bardin, A., and Primeau, F.: Tracing ventilation source of tropical pacific oxygen minimum zones with an adjoint global ocean transport model, Deep-Sea Research Part I: Oceanographic Research Papers, 139, 95-103, 2018.
Fuenzalida, R., Schneider, W., Garces-Vargas, J., Bravo, L., and Lange, C.: Vertical and horizontal extension of the oxygen minimum zone in the eastern South Pacific Ocean, Deep-Sea Res Pt Ii, 56, 1027-1038, 2009.
Garçon, V., Karstensen, J., Palacz, A., Telszewski, M., Aparco Lara, T., Breitburg, D., Chavez, F., Coelho, P., Cornejo-D'Ottone, M., Santos, C., Fiedler, B., Gallo, N. D., Grégoire, M., Gutierrez, D., Hernandez-Ayon, M., Isensee, K., Koslow, T., Levin, L., Marsac, F., Maske, H., Mbaye, B. C., Montes, I., Naqvi, W., Pearlman, J., Pinto, E., Pitcher, G., Pizarro, O., Rose, K., Shenoy, D., Van der Plas, A., Vito, M. R., and Weng, K.: Multidisciplinary Observing in the World Ocean's Oxygen Minimum Zone Regions: From Climate to Fish — The VOICE Initiative, Frontiers in Marine Science, 6, 2019.
Gnanadesikan, A., Dunne, J. P., and John, J.: Understanding why the volume of suboxic waters does not increase over centuries of global warming in an Earth System Model, Biogeosciences, 9, 1159-1172, 2012.
Hansell, D. A.: Recalcitrant dissolved organic carbon fractions, Annual review of marine science, 5, 421-445, 2013.
Johnson, K. S., Gordon, R. M., and Coale, K. H.: What controls dissolved iron concentrations in the world ocean?, Marine Chemistry, 57, 137-161, 1997.
Kalnay, E., Kanamitsu, M., Kistler, R., Collins, W., Deaven, D., Gandin, L., Iredell, M., Saha, S., White, G., Woollen, J., Zhu, Y., Chelliah, M., Ebisuzaki, W., Higgins, W., Janowiak, J., Mo, K. C., Ropelewski, C., Wang, J., Leetmaa, A., Reynolds, R., Jenne, R., and Joseph, D.: The NCEP/NCAR 40-year reanalysis project, B Am Meteorol Soc, 77, 437-471, 1996.
Kalvelage, T., Lavik, G., Jensen, M. M., Revsbech, N. P., Loscher, C., Schunck, H., Desai, D. K., Hauss, H., Kiko, R., Holtappels, M., LaRoche, J., Schmitz, R. A., Graco, M. I., and Kuypers, M. M.: Aerobic microbial respiration In oceanic oxygen minimum zones, PloS one, 10, 2015.
Kalvelage, T., Lavik, G., Lam, P., Contreras, S., Arteaga, L., Löscher, C. R., Oschlies, A., Paulmier, A., Stramma, L., and Kuypers, M. M. M.: Nitrogen cycling driven by organic matter export in the South Pacific oxygen minimum zone, Nature Geoscience, 6, 228-234, 2013.
Karstensen, J., Stramma, L., and Visbeck, M.: Oxygen minimum zones in the eastern tropical Atlantic and Pacific oceans, Progress in Oceanography, 77, 331-350, 2008.
Kuntz, L. B. and Schrag, D. P.: Hemispheric asymmetry in the ventilated thermocline of the Tropical Pacific, Journal of Climate 31, 1281-1288, 2018.
Levin, L. A.: Manifestation, Drivers, and Emergence of Open Ocean Deoxygenation, Annual review of marine science, 10, 229-260, 2018.
Libby, P. S. and Wheeler, P. A.: Particulate and dissolved organic nitrogen in the central and eastern equatorial Pacific, Deep-Sea Research Part I: Oceanographic Research Papers, 44, 345-361, 1997.
Llanillo, P. J., Pelegri, J. L., Talley, L. D., Pena-Izquierdo, J., and Cordero, R. R.: Oxygen Pathways and Budget for the Eastern South Pacific Oxygen Minimum Zone, Journal of Geophysical Research: Oceans, 123, 1722-1744, 2018.
Loginova, A. N., Thomsen, S., Dengler, M., Ludke, J., and Engel, A.: Diapycnal dissolved organic matter supply into the upper Peruvian oxycline, Biogeosciences, 16, 2033-2047, 2019.
Montes, I., Dewitte, B., Gutknecht, E., Paulmier, A., Dadou, I., Oschlies, A., and Garcon, V.: High-resolutionmodeling of the Eastern Tropical Pacific oxygen minimum zone: Sensitivity to the tropical oceanic circulation, Journal of Geophysical Research: Oceans, 119, 5515–5532, 2014.
Moreno, A. R., Garcia, C. A., Larkin, A. A., Lee, J. A., Wang, W. L., Moore, J. K., Primeaub, F. W., and Martiny, A. C.: Latitudinal gradient in the respiration quotient and the implications for ocean oxygen availability, PNAs, 117, 22866–22872, 2020.
Murtugudde, R., Seager, R., and Busalacchi, A.: Simulation of the tropical oceans with an ocean GCM coupled to an atmospheric mixed-layer model, Journal of Climate, 9, 1795-1815, 1996.
Niemeyer, D., Kriest, I., and Oschlies, A.: The effect of marine aggregate parameterisations on nutrients and oxygen minimum zones in a global biogeochemical model, Biogeosciences, 16, 3095-3111, 2019.

Oschlies, A., Brandt, P., Stramma, L., and Schmidtko, S.: Drivers and mechanisms of ocean deoxygenation, Nature Geoscience, 11, 467-473, 2018.
Oschlies, A., Koeve, W., Landolfi, A., and Kahler, P.: Loss of fixed nitrogen causes net oxygen gain in a warmer future ocean, Nature communications, 10, 2805, 2019.
Paulmier, A. and Ruiz-Pino, D.: Oxygen minimum zones (OMZs) in the modern ocean, Progress in Oceanography, 80, 113-128, 2009.
Pavia, F. J., Anderson, R. F., Lam, P. J., Cael, B. B., Vivancos, S. M., Fleisher, M. Q., Lu, Y., Zhang, P., Cheng, H., and Edwards, R. L.: Shallow particulate organic carbon regeneration in the South Pacific Ocean, Proceedings of the National Academy of Sciences of the United States of America, 116, 9753-9758, 2019.
Raimbault, P., Slawyk, G., Boudjellal, B., Coatanoan, C., Conan, P., Coste, B., Garcia, N., Moutin, T., and Pujo-Pay, M.: Carbon and nitrogen uptake and export in the equatorial Pacific at 150°W: Evidence of an efficient regenerated production cycle, Journal of Geophysical Research: Oceans, 104, 3341-3356, 1999.
Schmidtko, S., Stramma, L., and Visbeck, M.: Decline in global oceanic oxygen content during the past five decades, Nature, 542, 335-339, 2017.
Shigemitsu, M., Yamamoto, A., Oka, A., and Yamanaka, Y.: One possible uncertainty in CMIP5 projections of low-oxygen water volume in the Eastern Tropical Pacifi, Geophysical Research Letters, 31, 804-820, 2017.
Stramma, L., Johnson, G. C., Firing, E., and Schmidtko, S.: Eastern Pacific oxygen minimum zones: Supply paths and multidecadal changes, J Geophys Res-Oceans, 115, 2010.
Stramma, L., Johnson, G. C., Sprintall, J., and Mohrholz, V.: Expanding oxygen-minimum zones in the tropical oceans, Science, 320, 655-658, 2008.
Stramma, L., Oschlies, A., and Schmidtko, S.: Mismatch between observed and modeled trends in dissolved upper-ocean oxygen over the last 50 yr, Biogeosciences, 9, 4045-4057, 2012.
Sun, X., Frey, C., Garcia-Robledo, E., Jayakumar, A., and Ward, B. B.: Microbial niche differentiation explains nitrite oxidation in marine oxygen minimum zones, The ISME journal, 15, 1317-1329, 2021.
Talley, L. D., Feely, R. A., Sloyan, B. M., Wanninkhof, R., Baringer, M. O., Bullister, J. L., Carlson, C. A., Doney, S. C., Fine, R. A., Firing, E., Gruber, N., Hansell, D. A., Ishii, M., Johnson, G. C., Katsumata, K., Key, R. M., Kramp, M., Langdon, C., Macdonald, A. M., Mathis, J. T., McDonagh, E. L., Mecking, S., Millero, F. J., Mordy, C. W., Nakano, T., Sabine, C. L., Smethie, W. M., Swift, J. H., Tanhua, T., Thurnherr, A. M., Warner, M. J., and Zhang, J. Z.: Changes in ocean heat, carbon content, and ventilation: a review of the first decade of go-ship global repeat hydrography, Annual review of marine science, 8, 185-215, 2016.
Tanioka, T. and Matsumoto, K.: Stability of Marine Organic Matter Respiration Stoichiometry, Geophysical Research Letters, 47, 2020.
Van Mooy, B. A. S., Keil, R. G., and Devol, A. H.: Impact of suboxia on sinking particulate organic carbon: Enhanced carbon flux and preferential degradation of amino acids via denitrificatio, Geochimica et Cosmochimica Acta, 66, 457–465, 2002.
Wang, W. L., Moore, J. K., Martiny, A. C., and Primeau, F. W.: Convergent estimates of marine nitrogen fixation, Nature, 566, 205-211, 2019.
Wang, X. J., Behrenfeld, M., Le Borgne, R., Murtugudde, R., and Boss, E.: Regulation of phytoplankton carbon to chlorophyll ratio by light, nutrients and temperature in the Equatorial Pacific Ocean: a basin-scale model, Biogeosciences, 6, 391-404, 2009a.
Wang, X. J., Le Borgne, R., Murtugudde, R., Busalacchi, A. J., and Behrenfeld, M.: Spatial and temporal variations in dissolved and particulate organic nitrogen in the equatorial Pacific: biological and physical influences, Biogeosciences, 5, 1705-1721, 2008.
Wang, X. J., Murtugudde, R., Hackert, E., Wang, J., and Beauchamp, J.: Seasonal to decadal variations of sea surface pCO2 and sea-air CO2 flux in the equatorial oceans over 1984–2013: A basin-scale comparison of the Pacific and Atlantic Oceans, Global Biogeochemical Cycles, 29, 597-609, 2015.
Wang, X. J., Murtugudde, R., and Le Borgne, R.: Nitrogen uptake and regeneration pathways in the equatorial Pacific: a basin scale modeling study, Biogeosciences, 6, 2647-2660, 2009b.
Wanninkhof, R.: Relationship between wind speed and gas exchange over the Ocean, J Geophys Res-Oceans, 97, 7373-7382, 1992.

Ward, B. A., Wilson, J. D., Death, R. M., Monteiro, F. M., Yool, A., and Ridgwell, A.: EcoGEnIE 1.0: plankton ecology in the cGEnIE Earth system model, Geoscientific Model Development, 11, 4241-4267, 2018.
Weiss, R. F.: The solubility of nitrogen, oxygen and argon in water and seawater, Deep-Sea Research, 17, 721-735, 1970.
Williams, J. H. T., Totterdell, I. J., Halloran, P. R., and Valdes, P. J.: Numerical simulations of oceanic oxygen cycling in the FAMOUS Earth-System model: FAMOUS-ES, version 1.0, Geoscientific Model Development, 7, 1419-1431, 2014.
Wright, J. J., Konwar, K. M., and Hallam, S. J.: Microbial ecology of expanding oxygen minimum zones, Nature Reviews Microbiology, 10, 381-394, 2012.
Yu, J., Wang, X., Murtugudde, R., Tian, F., and Zhang, R. H.: Interannual‐to‐Decadal Variations of Particulate Organic Carbon and the Contribution of Phytoplankton in the Tropical Pacific During 1981–2016: A Model Study, Journal of Geophysical Research: Oceans, 126, 2021.
Zakem, E. J. and Levine, N. M.: Systematic Variation in Marine Dissolved Organic Matter Stoichiometry and Remineralization Ratios as a Function of Lability, Global Biogeochemical Cycles, 33, 1389-1407, 2019.

Tables

Table 1. Bias and root mean square error (RMSE) for DO (mmol m^{-3}) comparisons between WOA2013 and model simulations over 1991-2010 in the Eastern Tropical North Pacific (ETNP) and Eastern Tropical South Pacific (ETSP).

Layers	Statistics	Ref	Km6.9	Km18.7	Kb0.25	Kb0.5	Km6.9 Kb0.25	Km6.9 Kb0.5	Km18.7 Kb0.25	Km18.7 Kb0.5
ETNP (165°W-90°W, 5°N-20°N)										
200-400 m	Bias	-17.44	-14.84	-11.32	-16.34	-14.87	-13.51	-11.85	-9.71	-7.8
	RMSE	16.35	14.63	12.43	15.73	14.91	13.83	12.84	11.4	10.2
400-700 m	Bias	-16.35	-14.95	-12.51	-11.85	-7.5	-9.98	-5.39	-6.88	-2.04
	RMSE	10.6	9.83	8.45	8.26	6.73	7.49	6.38	6.5	6.78
700-1000 m	Bias	-9.22	-8.32	-5.99	-3.58	0.62	-2.71	1.38	-5.75	3.27
	RMSE	5.1	4.29	2.64	2.93	6.52	3.59	7.19	5.39	9.08
ETSP (110°W-80°W, 10°S-3°S)										
200-400 m	Bias	-7.09	-3.91	0.19	-6.43	-5.39	-2.84	-1.13	2.09	4.85
	RMSE	7.39	4.46	2.36	6.83	5.98	3.69	2.86	3.27	5.51
400-700 m	Bias	-11.3	-10.43	-7.94	-5.94	-0.88	-4.51	1.34	-1.21	5.23
	RMSE	12.98	12.15	10.06	8.52	6.03	7.41	5.65	5.81	7.38
700-1000 m	Bias	-7.3	-7.08	-5.13	-0.97	3.38	-0.62	3.94	1.05	5.46
	RMSE	12.82	12.49	11.22	8.98	8.63	8.76	8.68	8.59	9.34

Table 2. Volumes (10^{15} m^3) of suboxic and hypoxic water from WOA2013 and model simulations.

Regions	Waters	WOA2013	Reference	Km6.9	Km18.7	Kb0.25	Kb0.5	Km6.9 Kb0.25	Km6.9 Kb0.5	Km18.7 Kb0.25	Km18.7 Kb0.5
North Pacific	Suboxic	5.97	10.61	9.98	8.83	8.73	7.33	8.08	6.68	6.88	5.55
	Hypoxic	19.98	22.67	22.5	22.17	22.32	21.61	22.11	21.35	21.71	20.91
South Pacific	Suboxic	1.43	3.78	3.39	2.78	2.86	2.15	2.42	1.71	1.81	1.12
	Hypoxic	7.12	10.42	10.21	9.8	9.19	8.17	8.94	7.88	8.49	7.39

Suboxic: DO <20 mmol m^{-3}; Hypoxic: DO <60 mmol m^{-3}.

Figures

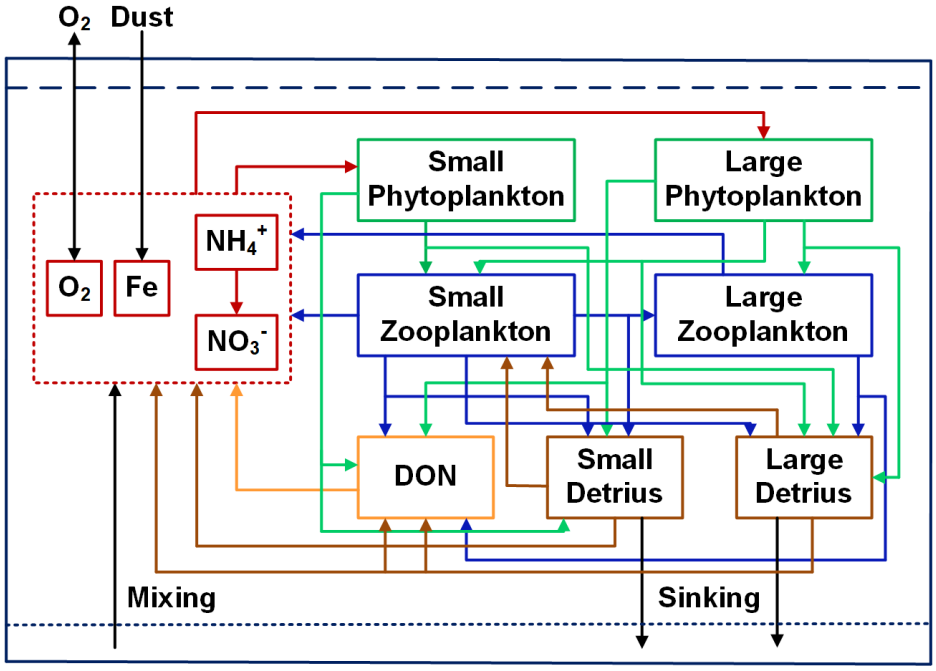

Figure 1. Flow diagram of ecosystem model. Red, green, blue, yellow and brown lines and arrows denote fluxes originating from inorganic forms, phytoplankton, zooplankton, DON and detritus, respectively.

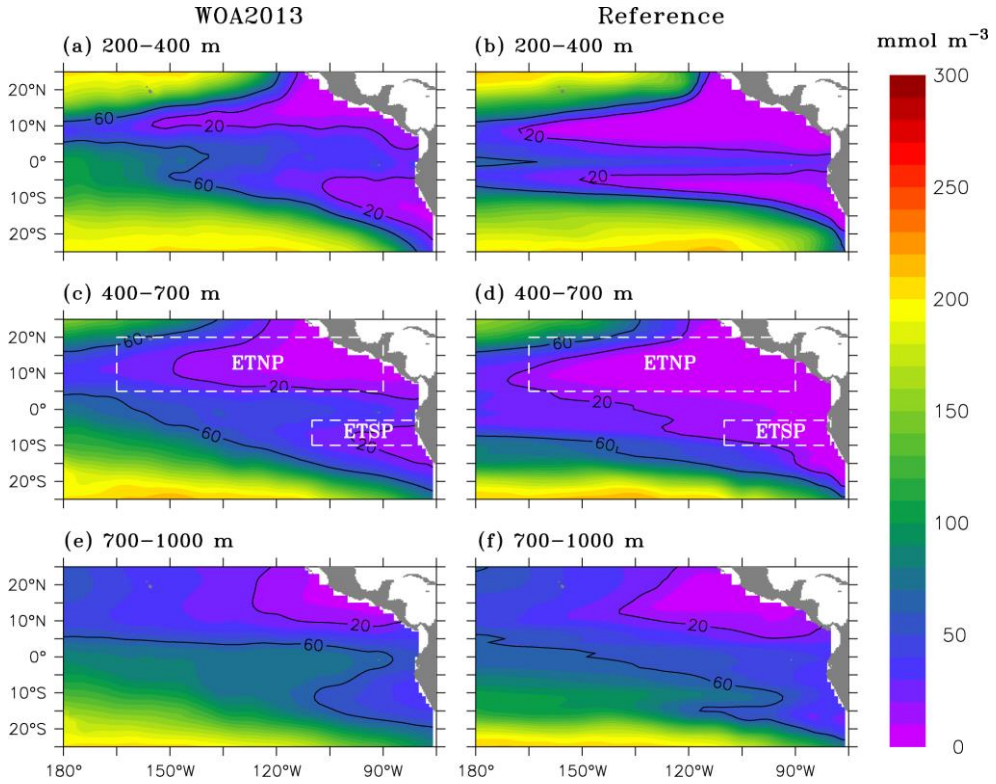

645 **Figure 2.** Comparisons of DO concentration between WOA2013 (left panel) and reference run (right panel) during 1991-2010. White dash lines in **(c)** and **(d)** denotes two boxes for ETNP (165°W-90°W, 5°N-20°N) and ETSP (110°W-80°W, 10°S-3°S).

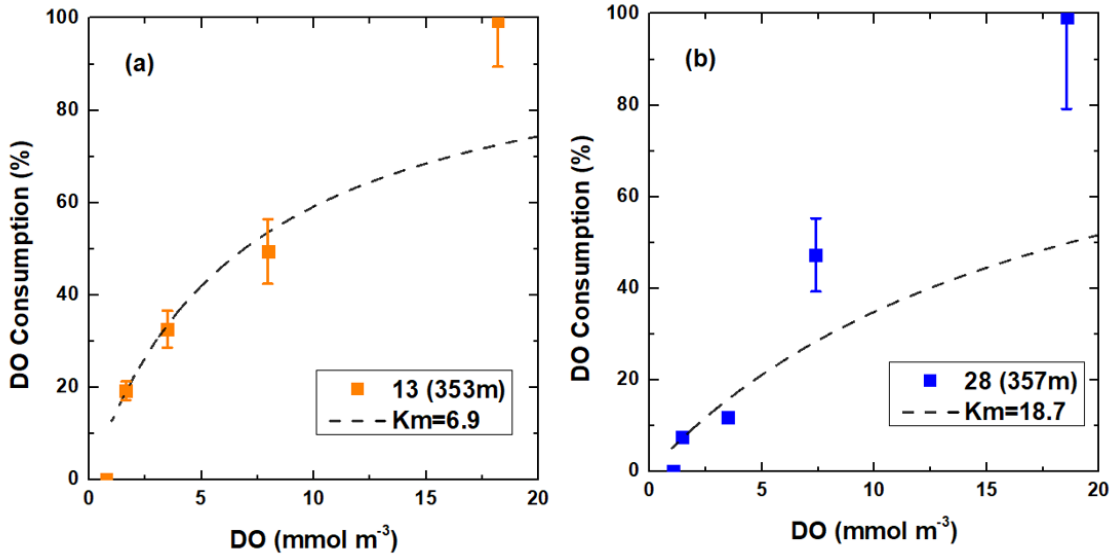

Figure 3. Biological consumption vs. DO concentration at (**a**) station 13 (353 m) and (**b**) station 28 (357 m) in the Peruvian OMZ. Data are from Kalvelage (2015).

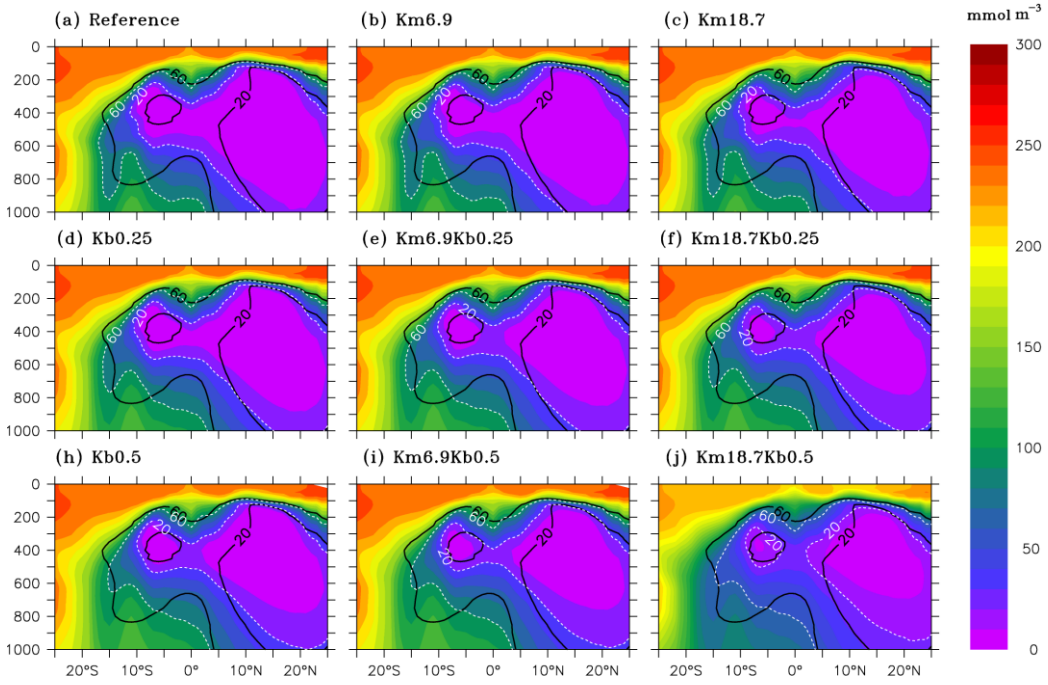

Figure 4. Vertical distribution of DO and asymmetric OMZs over 120°W-90°W from different model simulations for **(a)** reference run, **(b and c)** reduced O:C utilization ratio, **(d and h)** enhanced vertical mixing, and (**e, f, i, and j**) combination of reduced O:C utilization ratio and enhanced vertical mixing. Black lines denote contours of DO concentrations of 20 mmol m^{-3} and 60 mmol m^{-3} from WOA2013 data.

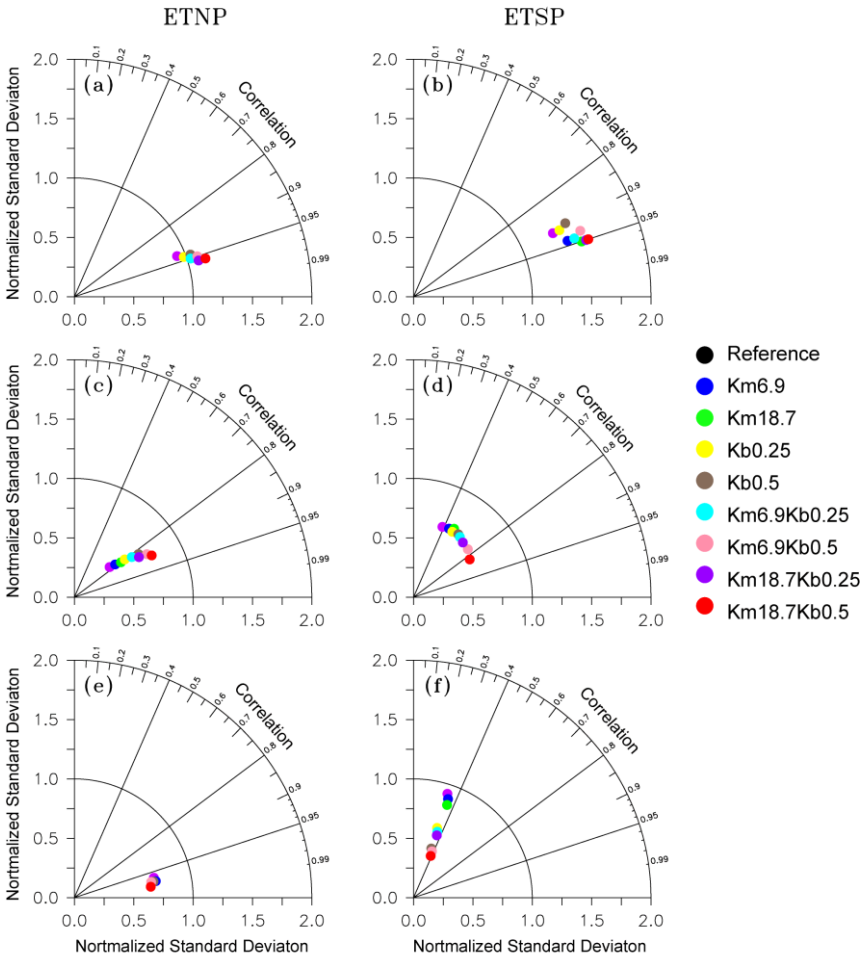

665 **Figure 5.** Taylor diagrams for the performance of simulated DO concentration (against WOA2013) from model simulations for ETNP (165°W-90°W, 5°N-20°N, left panel) and ETSP (110°W-80°W, 10°S-3°S, right panel) over **(a and b)** 200-400 m, **(c and d)** 400-700 m, and **(e and f)** 700-1000 m.

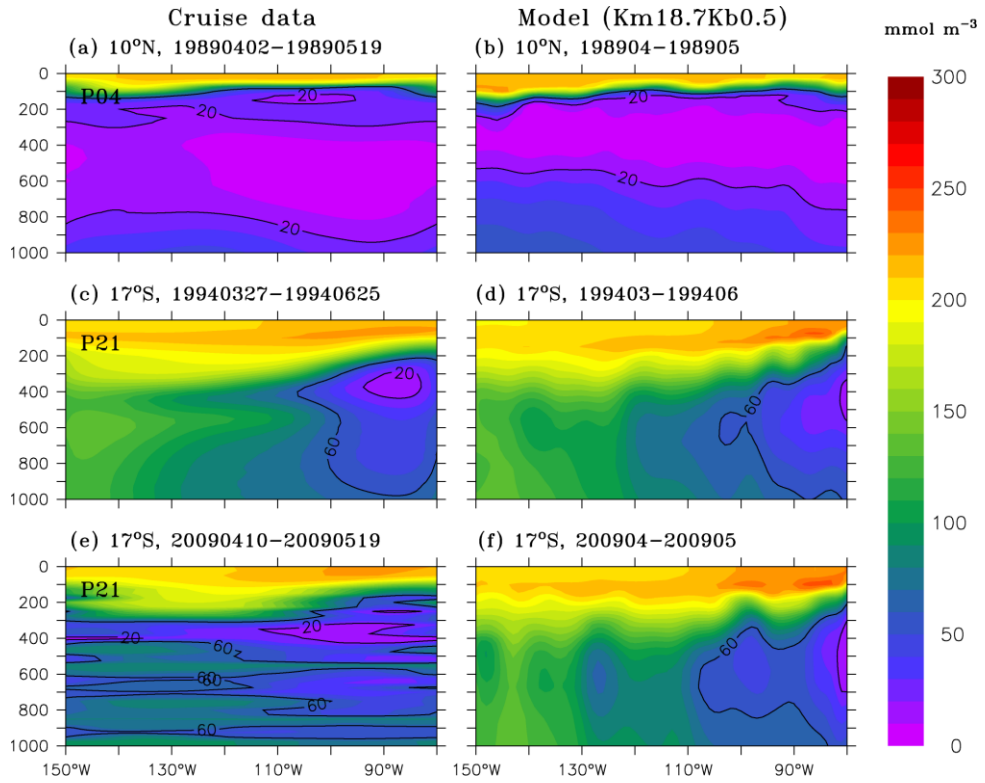

Figure 6. Distribution of DO from cruise data (left panel) and model simulation from the Km18.7Kb0.5 (see text for explanation; right panel). Observed DO along the P04 and P21 lines are from CCHDO (https://cchdo.ucsd.edu/).

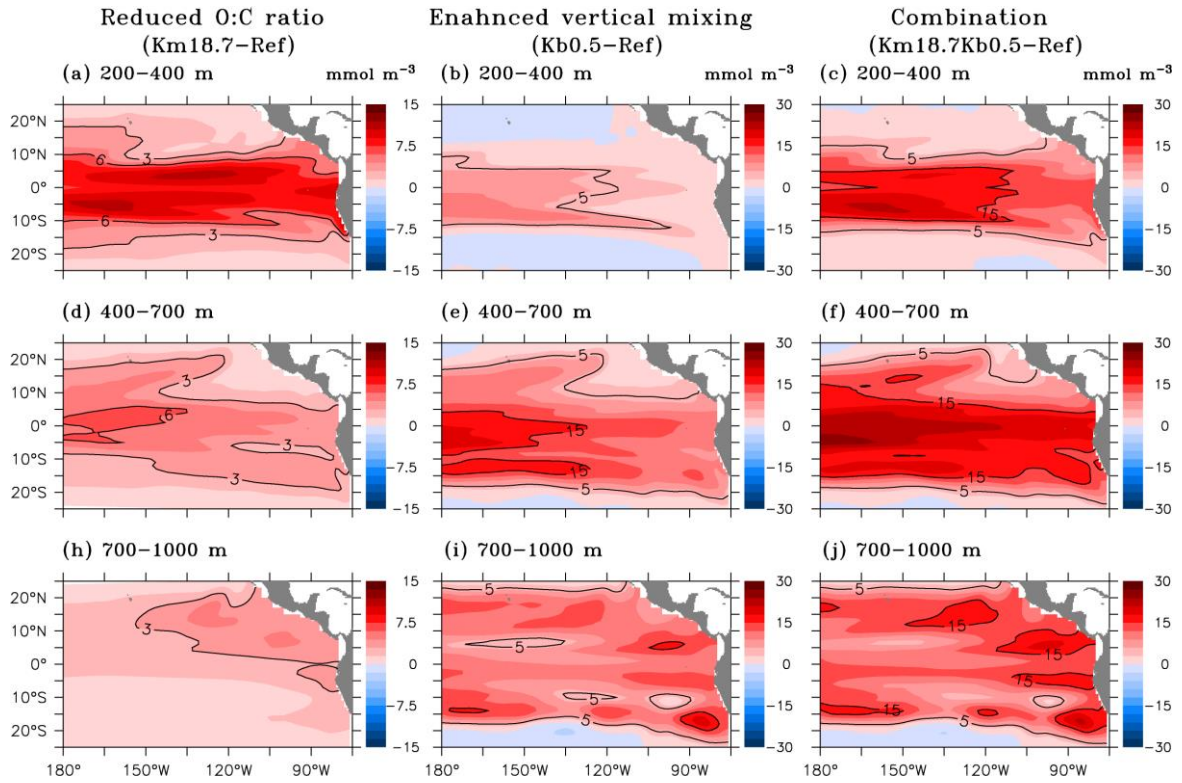

675

Figure 7. Changes of DO concentration averaged over **(a, b and c)** 200-400 m, **(d, e and f)** 400-700 m, and **(h, i and j)** 700-1000 m due to reduced O:C utilization ratio (left panel), enhanced vertical mixing (middle panel), and the combination of reduced O:C utilization ratio and enhanced vertical mixing (right panel).

680

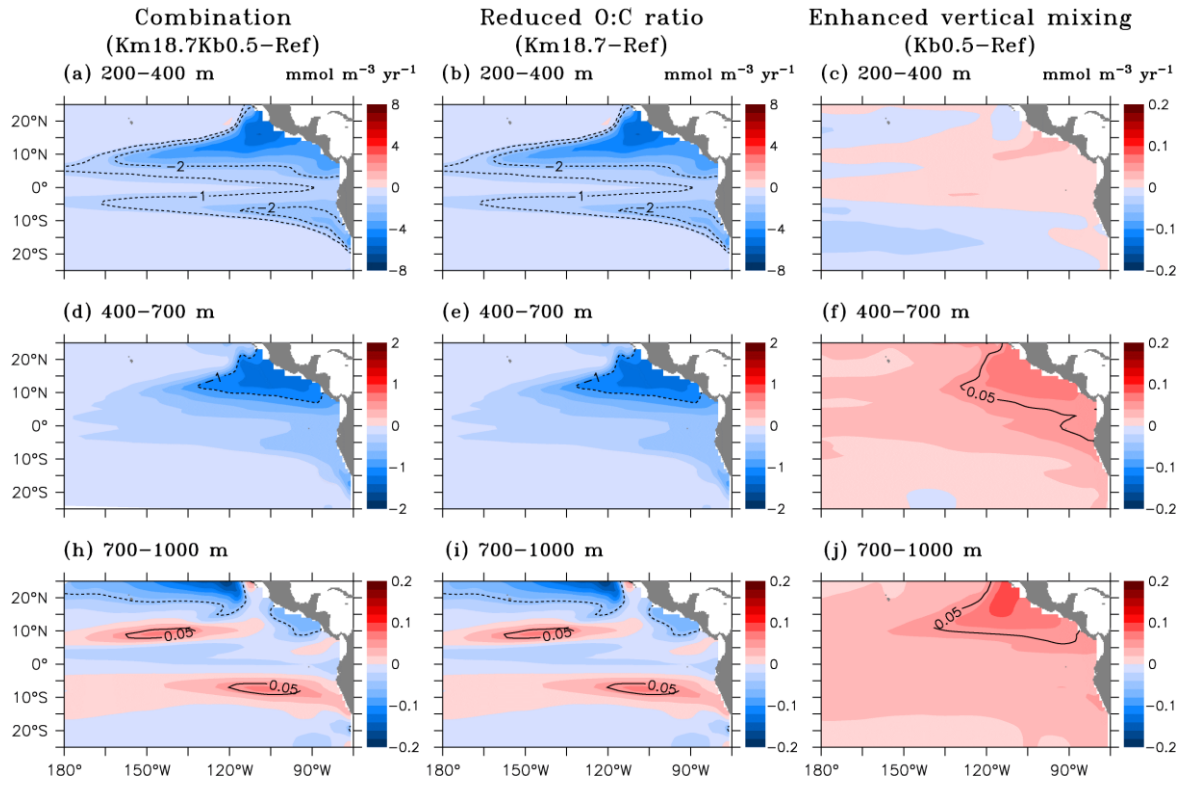

685 **Figure 8.** Changes in biological consumption over **(a, b and c)** 200-400 m, **(d, e and f)** 400-700 m, and **(h, i and j)** 700-1000 m due to the combination of reduced O:C utilization ratio and enhanced vertical mixing (left panel), reduced O:C utilization ratio (middle panel), and enhanced vertical mixing (right panel).

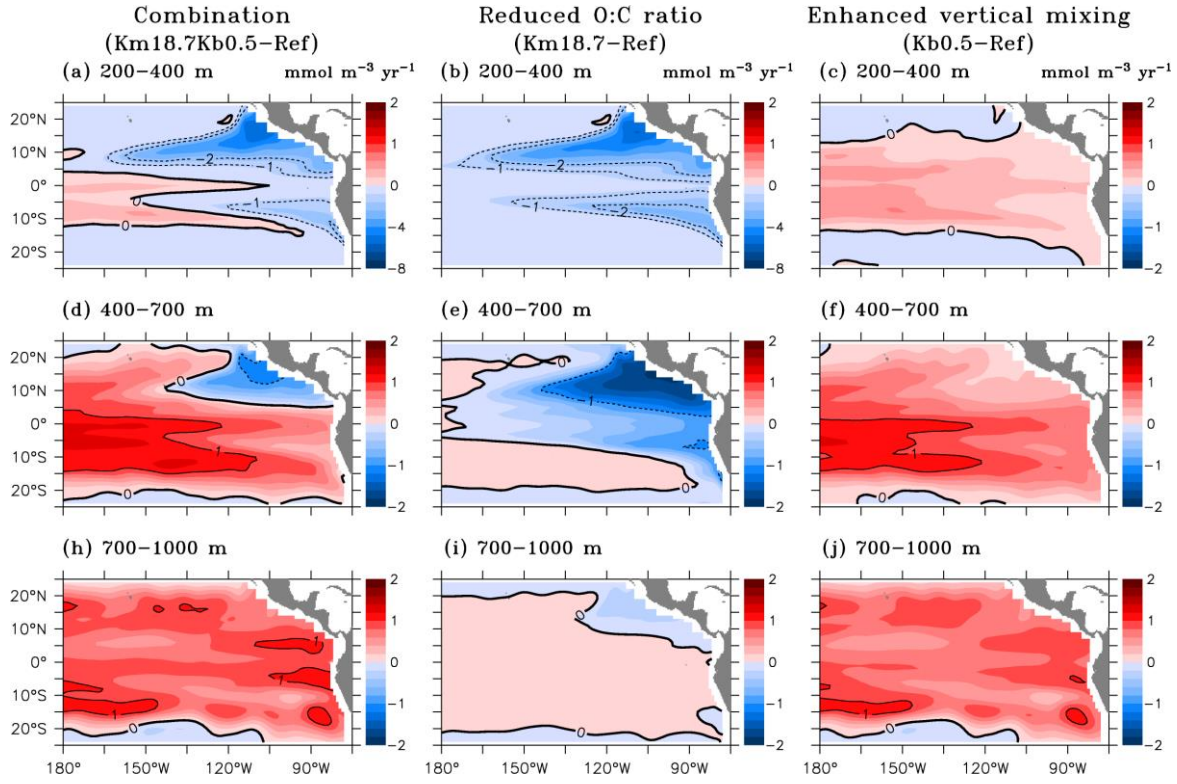

Figure 9. Changes in physical supply due to over **(a, b and c)** 200-400 m, **(d, e and f)** 400-700 m, and **(h, i and j)** 700-1000 m the combination of reduced O:C utilization ratio and enhanced vertical mixing (left panel), reduced O:C utilization ratio (middle panel), and enhanced vertical mixing (right panel).

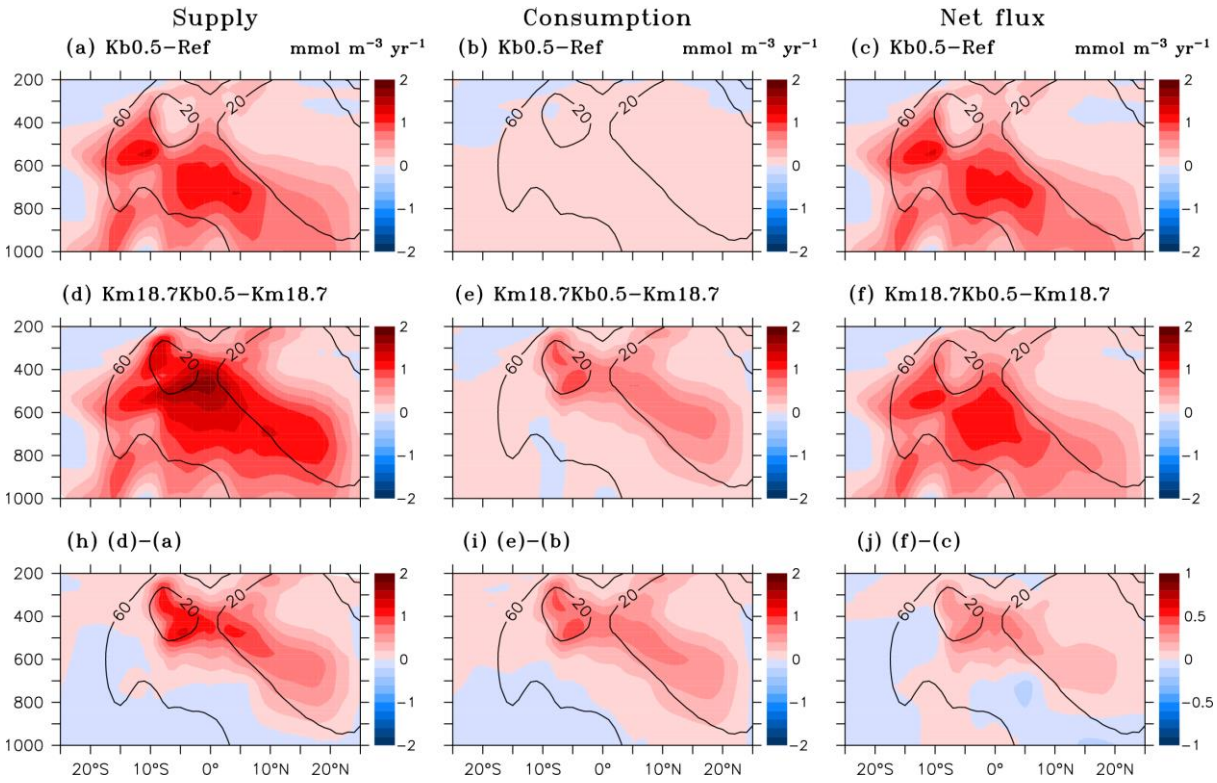

700 **Figure 10.** Changes in physical supply (left panel), biological consumption (middle panel), and net flux (right panel) under enhanced vertical mixing with **(d, e, and f, middle row)** and without **(a, b, and c, top row)** reduced O:C utilization ratio, and the differences between them (**h, i, and j, bottom row**).

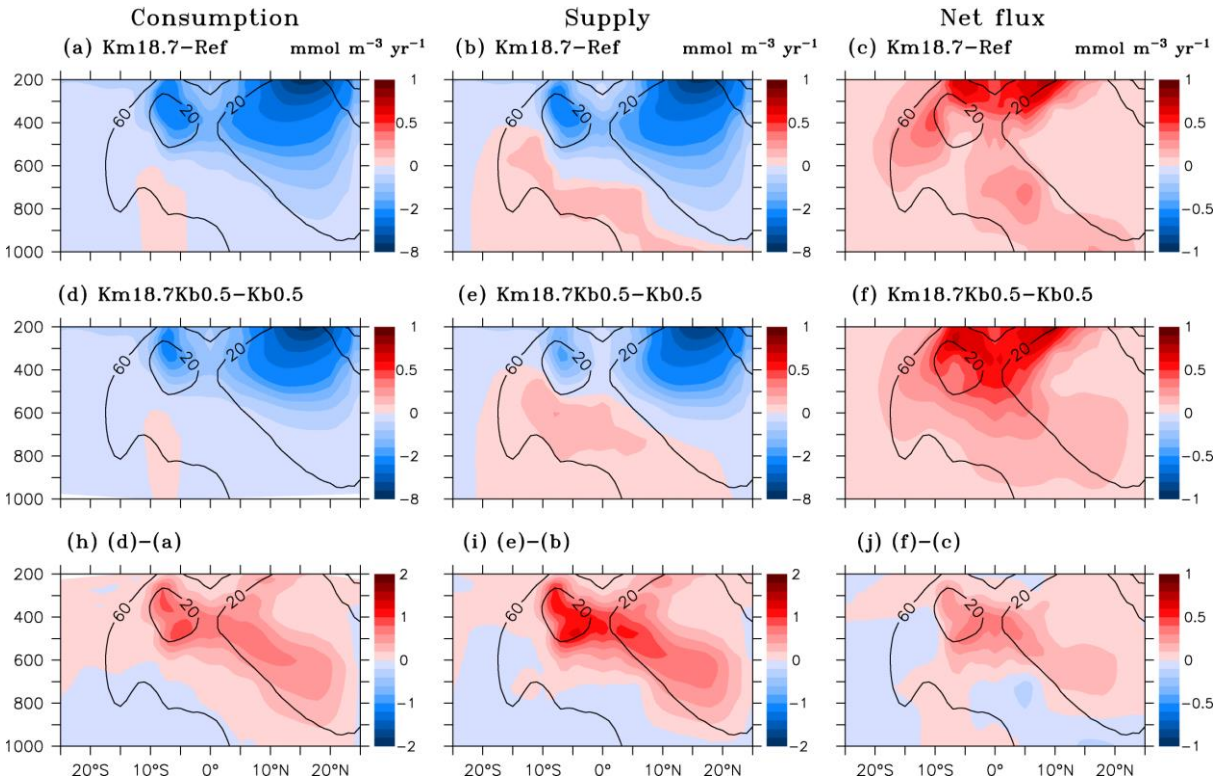

Figure 11. Changes in biological consumption (left panel), physical supply (middle panel), and net flux (right panel) under a reduced O:C utilization ratio with **(d, e, and f, middle row)** and without enhanced vertical mixing **(a, b, and c, top row)**, and the differences between them **(h, i, and j, bottom row)**.

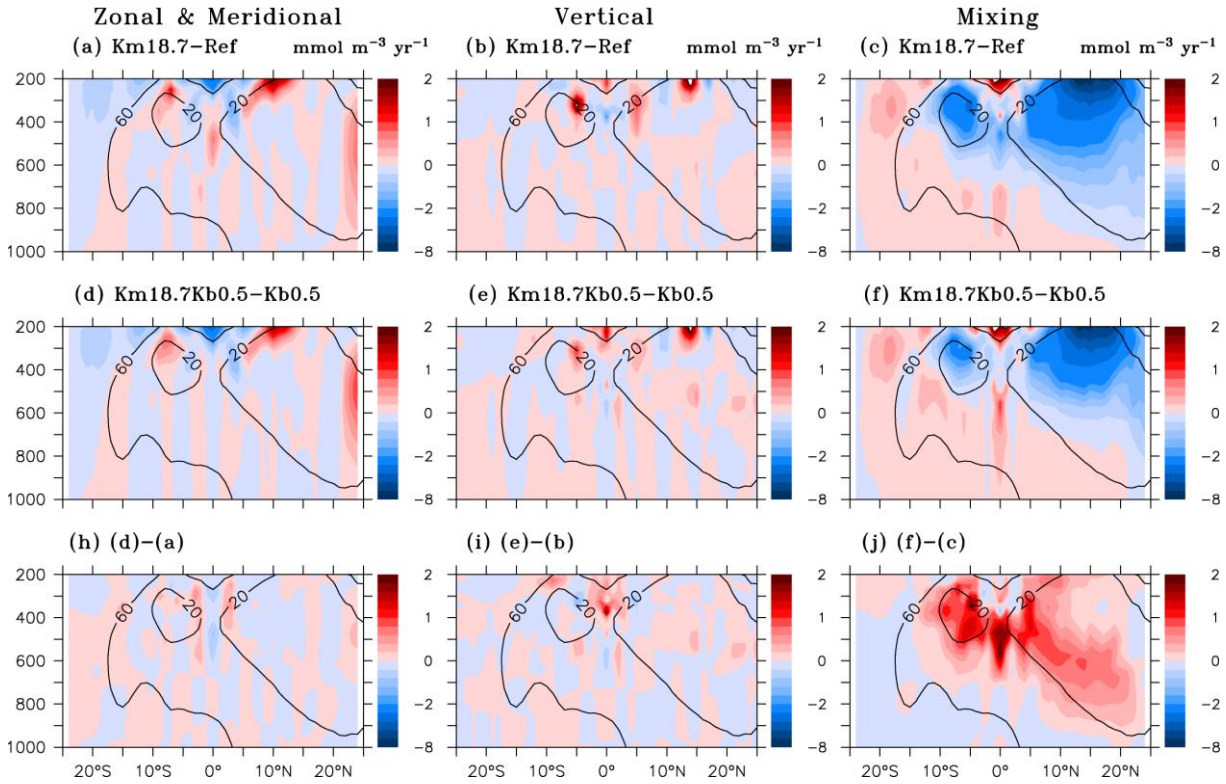

Figure 12. Changes and differences in zonal and meridional advections (left panel), vertical advection (middle pane), and vertical mixing (right panel) under a reduced O:C utilization ratio with **(d, e, and f, middle row)** and without enhanced vertical mixing **(a, b, and c, top row)**, and the differences between them **(h, i, and j, bottom row)**.